CAVITATION IN INJECTION NOZZLES
- EFFECT OF INJECTION PRESSURE FLUCTUATIONS -

Weixing Yuan, Günter H. Schnerr
Fachgebiet Strömungsmaschinen, Universität Karlsruhe (TH)
Kaiserstr. 12, D-76128 Karlsruhe, Germany
e-mail: guenter.schnerr@mach.uni-karlsruhe.de

Abstract

This work deals with a numerical simulation of the effect of injection pressure fluctuations on the cavitation processes in injection nozzles. The numerical approach is based on predicting the growth and collapse of bubbles in combination with a modified Volume-of-Fluid technique (VOF). A $k - \omega$ model is applied for turbulence modeling. Calculations confirm that there exists phase shift among the time history of the injection pressure, the transient velocity, and the cavitation process.

1   Introduction

Phase shift and time delay are typical for unsteady fluid dynamics. They certainly also appear in injection nozzle flows. Experimental investigations (see Chaves et al., 2000) and numerical simulations (see Yuan & Schnerr, 2001) have confirmed, that there exists a phase shift between the time history of the injection pressure and the cavitation process in injection nozzles. This complex process will modulate the flow condition at the nozzle exit, which affects the spray structure and the atomization process. Unfortunately, it is very difficult to produce transparent nozzles of realistic dimensions of the order of $10^{-4} - 10^{-3}$m. Scaled-up models of real injectors can not be used for flow visualization and measurement, because cavitation has its own length scale and it is not possible to scale it up. This length scale is determined by the characteristic collapse time of a given cavity and the flow velocity which can be of the order of several hundred meters per second.

Because of the difficulties performing experiments for this small scale flow, time accurate numerical solutions of flows through injection nozzles are of great interest. Numerical simulation provides an efficient method to further understand this small scale flow. In this study we will first briefly describe our numerical method for the simulation of cavitating flows, and then we use the method to predict the dynamic performance of cavitating flows in injection nozzles due to supply pressure fluctuations. The present numerical approach to the solution of cavitation is based on a combination of the Volume-of-Fluid technique (VOF) (Hirt & Nichols, 1981) with an additional model for the growth and collapse of bubbles (Rayleigh, 1917). The calculations show, that the cavitation process depends on the dynamic condition of the inlet pressure. A transient rise of the nozzle inlet pressure forces cavitation to recede and a sharp decrease of the injection pressure enhances cavitation.

2   Mathematical and numerical formulation

The vapor-liquid flow is treated as a homogeneous bubble-liquid mixture, hence only one set of equations is used for description. The governing equations are

$$\frac{\partial \varrho}{\partial t} + \mathrm{div}(\varrho \vec{c}) = 0, \tag{1}$$

$$\frac{\partial(\varrho \vec{c})}{\partial t} + \mathrm{div}[\varrho \vec{c}\vec{c} + (p + \frac{2}{3}\mu\ \mathrm{div}\vec{c})\ \overset{\Rightarrow}{I}] = 2\mu\ \mathrm{div}\ \overset{\Rightarrow}{D}, \tag{2}$$

where t stands for the time, $\vec{c}$ for the velocity, p for the static pressure. $\overset{\Rightarrow}{I}$ is the unit tensor and $\overset{\Rightarrow}{D}$ is the rate of strain (deformation) tensor. The equations of motion are constructed with the constitutive relations

for the density ϱ and the dynamic viscosity μ:

$$\varrho = (1 - \alpha)\varrho_l + \alpha\varrho_v, \quad \mu = (1 - \alpha)\mu_l + \alpha\mu_v, \tag{3}$$

where α is the vapor fraction. The subscripts $_l$ and $_v$ stand for the properties of pure liquid and pure vapor which are assumed to be constant. In the calculations μ_{eff} is used instead of the molecular viscosity μ:

$$\mu_{eff} = \mu + \mu_t, \tag{4}$$

where μ_t represents the turbulence viscosity which is modeled using the $k - \omega$ model introduced by Wilcox (1998). The liquid and the vapor share the same turbulence viscosity. Interested reader may refer to our previous work (Yuan et al. 2000).

To close the system of equations, an additional relation is needed, since we have introduced a new variable α. As proposed by Schnerr and Sauer (2001), the vapor is assumed to consist of mini spherical bubbles. Therefore, the vapor fraction can be calculated by

$$\alpha = \frac{V_{Vapor}}{V_{Liquid} + V_{Vapor}} = \frac{n_0 \cdot \frac{4}{3}\pi R^3}{1 + n_0 \cdot \frac{4}{3}\pi R^3}, \tag{5}$$

where R is the bubble radius and n_0 is defined as nuclei concentration per unit volume of pure liquid. The Rayleigh relation (Rayleigh, 1917) is used for description of the bubble growth:

$$\dot{R} = \frac{dR}{dt} = \sqrt{\frac{2}{3}\frac{p(R) - p_\infty}{\varrho_l}}, \tag{6}$$

where $p(R)$ is the pressure in the liquid at the bubble boundary and p_∞ is the pressure at a large distance from the bubble. This relation is applicable in the range of moderately low pressures. In this study, $p(R)$ is set equal to the equilibrium vapor pressure $p_{vap}(T)$ and p_∞ to the ambient pressure in the computational cell. Using this assumption we can calculate the vapor production rate from the following equation

$$\frac{d\alpha}{dt} = (1 - \alpha)\frac{4\pi n_0 R^2 \dot{R}}{1 + n_0 \cdot \frac{4}{3}\pi R^3}. \tag{7}$$

To overcome numerical difficulties due to the strong variation of the density between the liquid and vapor phase, as proposed by Spalding (1974) and Schnerr & Sauer (2001), we reformulate the continuity equation (Eq. 1) in another manner:

$$\nabla \cdot \vec{c} = \frac{-1}{\varrho}\left(\frac{\partial\varrho}{\partial t} + \vec{c} \cdot \nabla\varrho\right) = \frac{-1}{\varrho}\frac{d\varrho}{dt} = \frac{\varrho_l - \varrho_v}{\varrho}\frac{d\alpha}{dt}. \tag{8}$$

For two-phase systems with high density ratios this form is much more suitable for numerical calculations, because $\vec{c}$ is by definition continuous at the cell interface. This nonconservative form of the continuity equation is solved together with the momentum equation (Eq. 2) by a pressure correction method, here a modified SIMPLE algorithm. For the vapor fraction α we derive the following transport equation which is a variant of the continuity equation (Eq. 1) together with Eqs. 7, 8:

$$\frac{\partial\alpha}{\partial t} + \nabla \cdot (\alpha\vec{c}) = \frac{d\alpha}{dt} + \alpha \nabla \cdot \vec{c} = \frac{(1 - \alpha)\varrho_l}{(1 - \alpha)\varrho_l + \alpha\varrho_v}\frac{n_0}{1 + n_0 \cdot \frac{4}{3}\pi R^3}\frac{d}{dt}\left(\frac{4}{3}\pi R^3\right). \tag{9}$$

The formulation of the numerical solution procedure is based on a cell-centered finite-volume method for the variables, e.g. for $u, v, p, k, \omega, \alpha$. The calculations are performed by first computing the vapor transportation (Eq. 9) for the new time step, and then using the new vapor fraction, i.e., the new mixture density, to calculate the momentum equations of the flow. Both inflow and outflow boundaries are modeled as specified pressure surfaces.

3 Computed results

In this study we are going to further investigate the effect of injection pressure fluctuations on cavitation processes in injection nozzles. The physical reason for the pressure fluctuation is the so-called "water hammer" in the needle chamber. We use our numerical code to calculate the cavitating flows under periodic inlet

pressure conditions. The selected geometry is the nozzle of Roosen et al. (1996). The nozzle hole consists of a rectangular-shaped channel of $0.2 \times 0.28 \times 1\text{mm}^3$ (width $\times$ height $\times$ length). In order to reduce the computational time, a 2-D flow and symmetry with respect to the nozzle axis is assumed, see figure 1. The interaction between the internal and external flow is not taken into account. Therefore, the nozzle exit is simply specified as a constant pressure surface, here $p_{Exit} = 21\text{bar}$, which was used by Roosen et al. (1996) for their experimental observations.
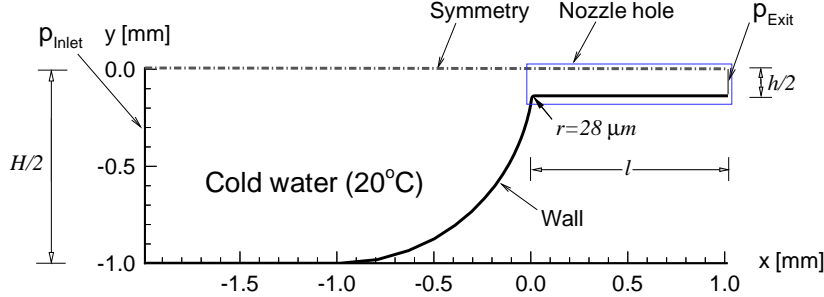
Figure 1: Lower half of the 2-D plane injection nozzle.

Inception of cavitation in a liquid requires the presence of nuclei. Variations of the nuclei concentration and the nuclei radii have been performed in our previous work, see Yuan et al. (2000). The computed results using the nuclei concentration $n_0 = 1.5 \times 10^{14} \frac{\text{nuclei}}{m^3 \text{water}}$ and the nuclei radius $R_0 = 0.3 \mu m$ for the cases with $p_{Injection} = 80\text{bar}$, $p_{Exit} = 21\text{bar}$ and $p_{Injection} = 80\text{bar}$, $p_{Exit} = 11\text{bar}$ agree very well with the experimental observations of Roosen et al. (1996). These values of nuclei will be used in this study, which corresponds to a small initial vapor fraction $\alpha_0 = 0.0017\%$.

3.1 Cavitation diminution/enhancement due to rapid increase/decrease of injection pressure

For constant pressure boundary conditions, experimental observations (see e.g. Chaves et al., 1995) and numerical investigations (Yuan & Schnerr, 2001) have confirmed that higher constant injection pressures cause larger cavitation regions. The physical reason is that, for steady flow, higher inlet pressure causes higher velocities and consequently higher tensile stress (negative pressure) at the throat of the nozzle. The lower negative pressure enhances the cavitation. However, when the inlet pressure is unsteady, the transient cavitation process differs significantly from steady flow. The pressure wave spreads out with the speed of sound, which is infinite for the incompressible liquid in the non-cavitated region, whilst the flow velocity changes with a time delay due to the time derivative in the momentum conservation (Eq. 2). This time delay leads to a phase shift between the time history of the inlet pressure and the transient velocity. If the inlet pressure increases, the pressure in the nozzle rises simultaneously, which forces the vapor bubbles to collapse, such that the extension of the cavitation region becomes smaller. On the other hand, the sharp decrease of the inlet pressure enhances the cavitation. Therefore, the most intense cavitation does not unconditionally form at the highest transient inlet pressure, when the inlet pressure increases and decreases rapidly, see Yuan & Schnerr (2001).

To further investigate this completely contrary cavitation behaviour to what occurs for steady flow, we start with the assumption of a periodic square wave inlet pressure $p = 80\text{bar} \pm 10\text{bar}$ applied to the nozzle of Roosen et al. (1996). The amplitude $A_p = 10\text{bar}$ is assumed such that neither super cavitation nor hydraulic flip situations occur, which simplifies the outlet boundary conditions. Simultaneous pressure measurements in the needle chamber (5mm from the nozzle) indicate that the fluctuation frequency can be of the order of $25\text{kHz} - 55\text{kHz}$, see e.g. Chaves and Obermeier (1996). Grabitz et al. (1995) used sinusoidal pressure fluctuations in front of the nozzle with a frequency $f = 37\text{kHz}$ for their experimental and numerical investigations of the liquid jets after a small scale nozzle. This realistic frequency $f = 37\text{kHz}$ is chosen in this study. The assumed square wave inlet pressure and the calculated total vapor volume as well as the mass flow rate are shown in figures 2 and 3 (top). The flow rate is integrated at the nozzle exit. The computed unsteady periodic vapor fraction distribution is depicted in figure 4.

Figure 4 ($f = 37\text{kHz}$) displays: When the inlet pressure jumps from 70bar to 90bar, the rise of the pressure in the nozzle forces the cavitation region to recede. It can be expected that the cavitation in injection nozzles disappears for a short-time, provided that the amplitude of the injection pressure fluctuation is large enough. On the other hand, when the inlet pressure steps down from 90bar to 70bar, the pressure in the nozzle decreases dramatically, which forces the vapor bubbles to grow. This process differs significantly from steady flow. This unsteady effect is also verified by figure 2 (top) which shows the change of the total vapor
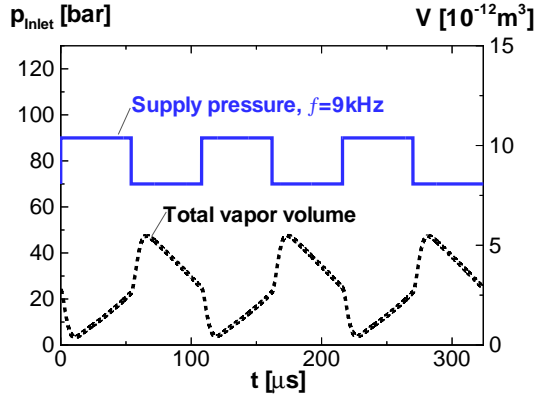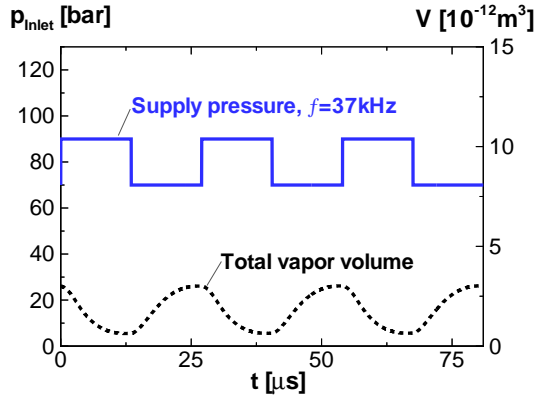
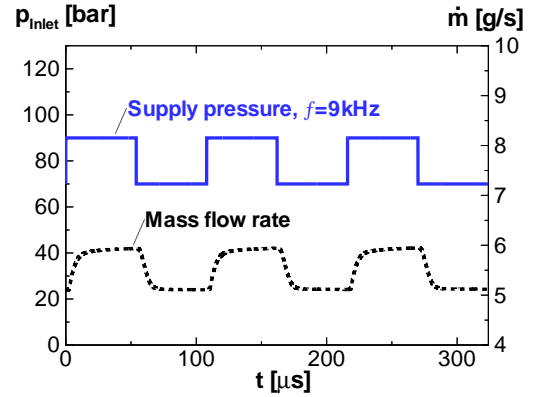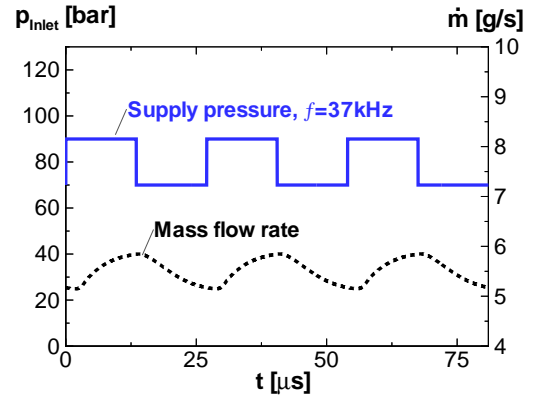Figure 2: Total vapor volume variation depending on inlet pressure frequency. **Square wave** inlet pressure, $p_{Exit} = 21$bar = const..

Figure 3: Mass flow rate variation depending on inlet pressure frequency. **Square wave** inlet pressure, $p_{Exit} = 21$bar = const..

volume in the nozzle versus time. Because of the short duration of one cycle, the cavitation region does not become more intense again, during the partial constant stage of the inlet pressure $p_{Inlet}(t) = 90bar$.

3.2 Cavitation intensification/weakening afresh after a short duration of partial constant stage of inlet pressure

As mentioned above, when the inlet pressure increases rapidly, the pressure at the throat of the nozzle rises due to the time derivative in equation 2, until the liquid in the nozzle is accelerated. It means if the duration of the partial constant stage of the inlet pressure is larger than the time needed for the acceleration of the liquid, the pressure at the throat on the nozzle decreases again and consequently the cavitation becomes more intense. To investigate the effect of the cycle length of the inlet pressure fluctuations, or in other words the effect of the frequency of inlet pressure fluctuations, we reduce the frequency to $f = 9kHz$. The amplitude remains unchanged with $A_p = 10bar$. The assumed inlet pressure and the calculated total vapor volume as well as the mass flow rate are shown together with those of $f = 37kHz$ in figures 2 and 3. The computed unsteady periodic vapor fraction distribution is depicted in figure 5.

We recognize that the rise of the pressure in the nozzle forces the cavitation region to recede, when the inlet pressure jumps from 70bar to 90bar, see figure 5. It has been shown under the condition with $f = 37$kHz, see figure 4. However, as shown in figure 5, after a time interval (here about T/8), the cavitation begins to be more intense. This is because, the velocity of the fluid becomes higher after this time interval, such that the pressure at the throat of the nozzle decreases and consequently drives the cavitation to be more intense. This intensification of the cavitation development does not occur under the condition with $f = 37$kHz because of its short duration of the cycle. If the inlet pressure does not change once again, the cavitation region will extend toward the nozzle exit, see Yuan & Schnerr (2001). However, when the inlet pressure steps down from 90bar to 70 bar, the pressure in the nozzle decreases dramatically, which forces the vapor bubbles to grow. This growth process continues only for a short-time (here ca. T/8). Thereafter, the cavitation region becomes smaller as the velocity at the throat of the nozzle decreases once again. Certainly, the cavitation region will become very small if the inlet pressure remains constant at 70bar.
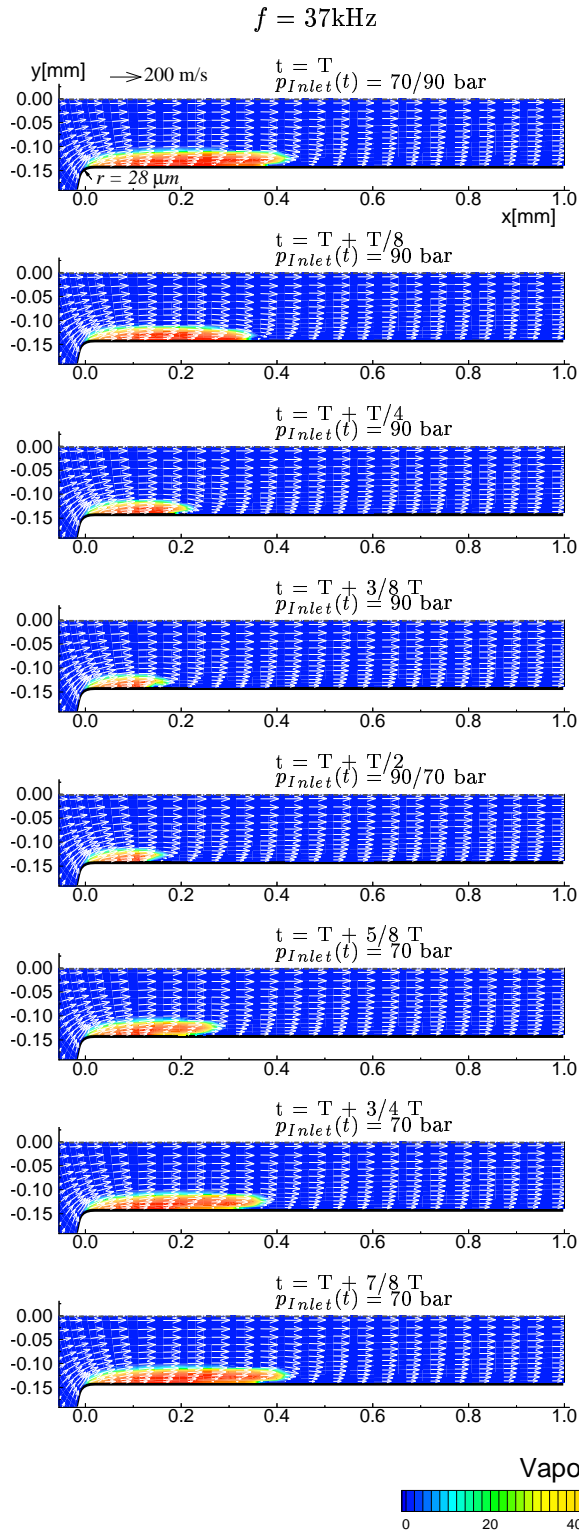
Figure 4: Unsteady periodic vapor fraction distribution, **square wave** inlet pressure $p_{Inlet}(t)$, $f = 37\text{kHz}$, $p_{Exit} = 21\text{bar} = \text{const.}$.
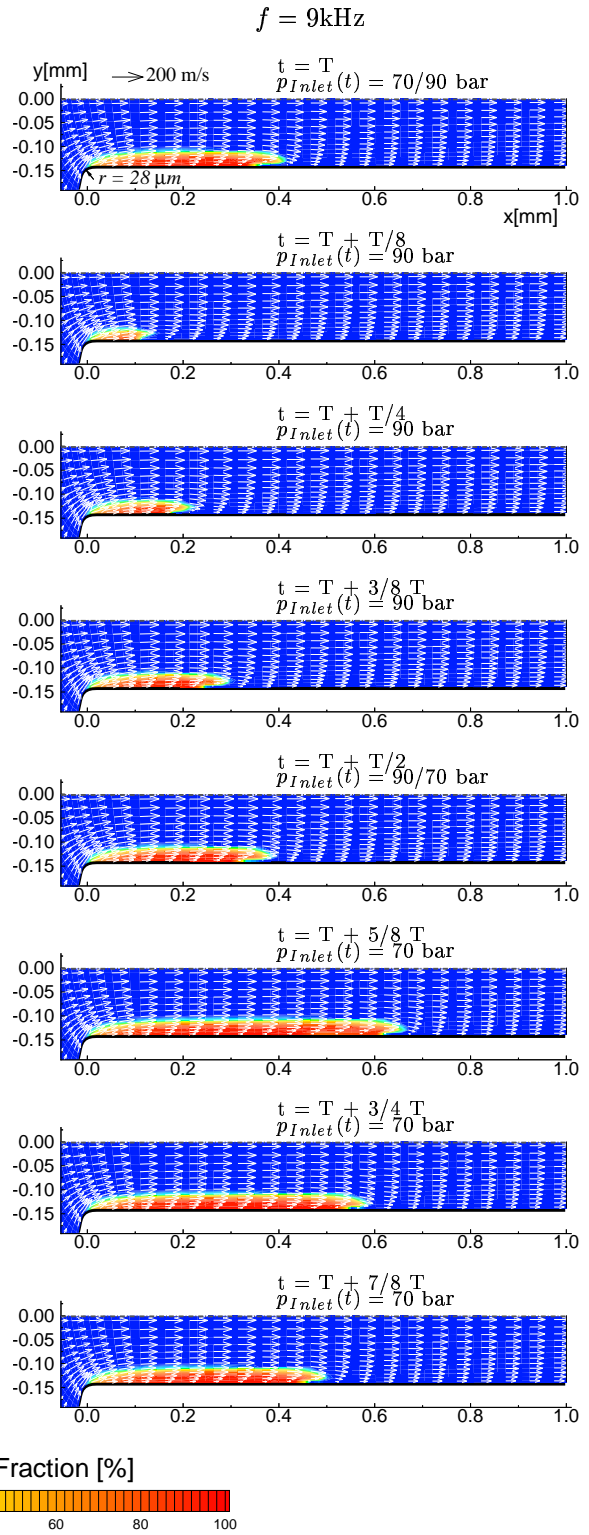
Figure 5: Unsteady periodic vapor fraction distribution, **square wave** inlet pressure $p_{Inlet}(t)$, $f = 9\text{kHz}$, $p_{Exit} = 21\text{bar} = \text{const.}$.

The time history of the inlet pressure and the transient velocity (mass flow rate) shown in figure 3 (bottom) indicate that a time delay about T/2 for the case $f = 37$kHz and T/8 for $f = 9$kHz exists, till the flow velocity reaches the threshold values corresponding to the maximum or minimum inlet pressure, respectively. This implies that the two cases have the same absolute time interval for the acceleration of the liquid. This time interval should be controlled by the momentum conservation (Eq. 2), which is dominated by the non-cavitated single phase flow. Corresponding to this time delay, the cavitation begins to become more intense or weaker after the flow is accelerated or decelerated, respectively, see figure 2.

3.3   Cavitation behavior due to different types of injection pressure fluctuations

Analysis of the vapor transport equation 9 shows that the cavitation process is determined by local pressure (local effect) as well as the transport velocity (convective effect). On the other hand, due to the mass transfer and the displacement of the phase interfaces, the cavitation development modulates the flow field, see equation 8. It is difficult to separate the interactions from each other. An indirect way is to vary the type of injection pressure fluctuations to get different pressure and velocity fields. Here, we perform test cases with triangle wave inlet pressures instead of the square wave inlet pressures. The frequencies $f = 37$kHz and $f = 9$kHz are chosen. The amplitude also remains at $A_p = 10$bar. The computed total vapor volume and the mass flow rate are shown in figures 6 and 7, the corresponding vapor fraction distributions in figures 8, 9.
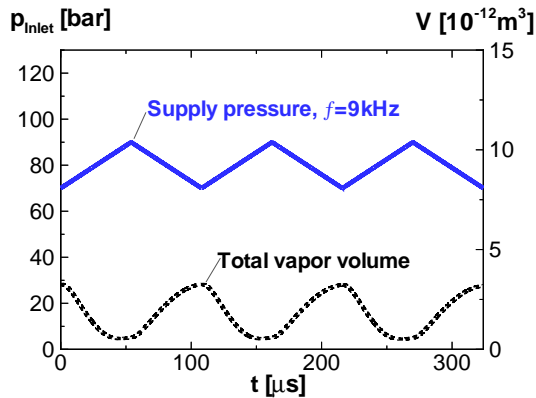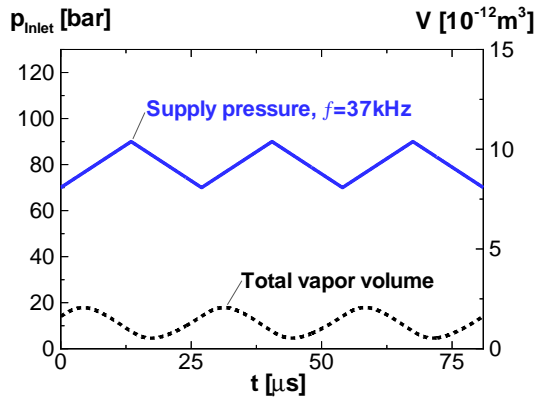

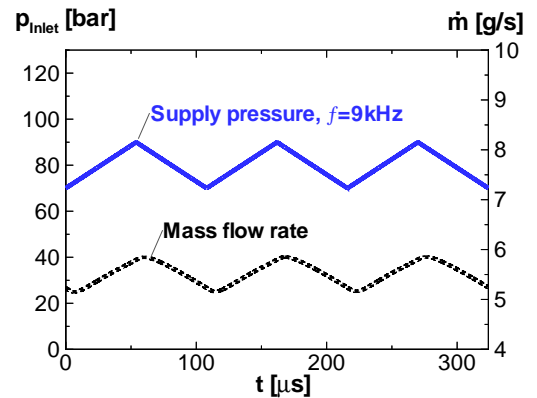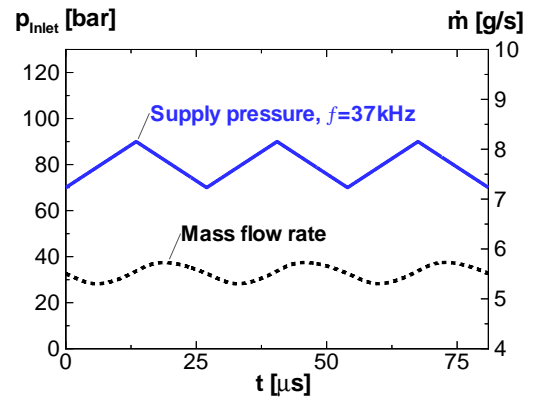Figure 6: Total vapor volume variation depending on inlet pressure frequency. **Triangle wave** inlet pressure, $p_{Exit} = 21$bar = const..

Figure 7: Mass flow rate variation depending on inlet pressure frequency. **Triangle wave** inlet pressure, $p_{Exit} = 21$bar = const..

Figure 7 shows the phase shift between the time history of the inlet pressure and the transient velocity. Corresponding to it, a phase shift of the cavitation process exists, see figure 6. However, the phase shift of the cavitation differs significantly from that of the transient velocity. It indicates that the cavitation has its own time scale. Because of the nonlinearity of the governing equetions, no explicit condition relating the time history of the inlet pressure, the transient velocity and the cavitation has been obtained.

Comparisons of figure 8 with figure 4 and figure 9 with figure 5 show that the cavitation processes under the conditions with triangle wave inlet pressures differ significantly from those with the square wave inlet
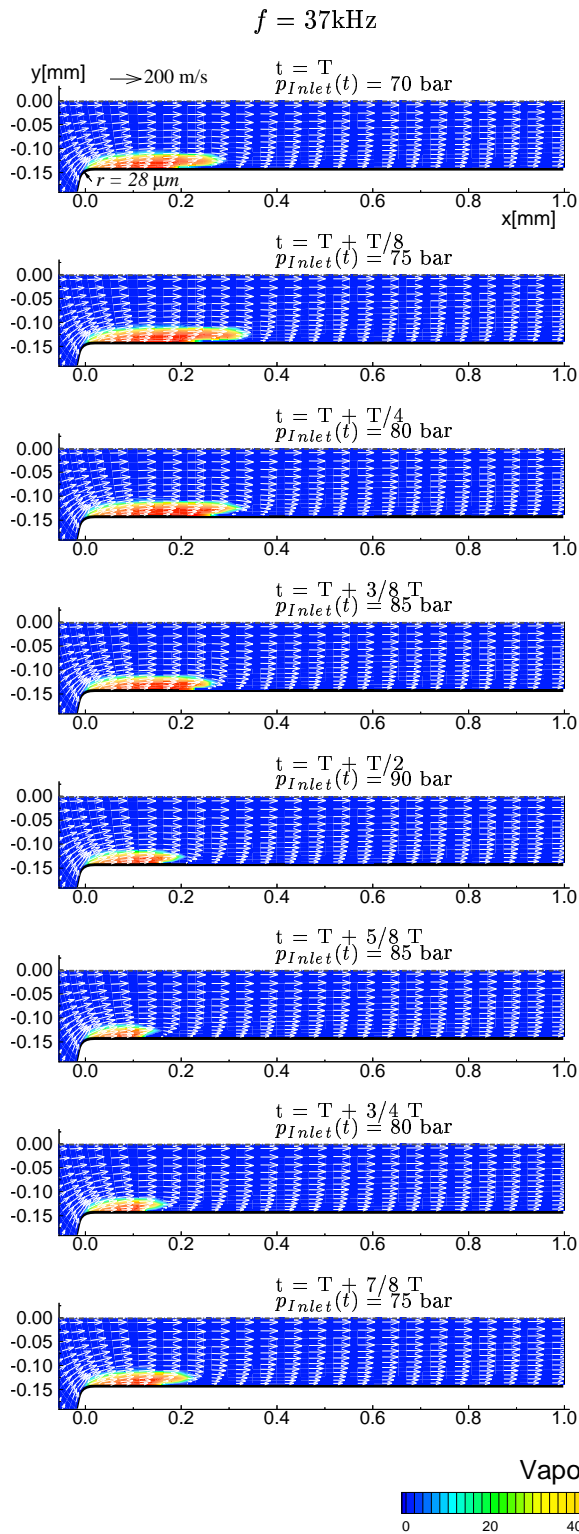
Figure 8: Unsteady periodic vapor fraction distribution, **triangle wave** inlet pressure $p_{Inlet}(t)$, $f = 37$kHz, $p_{Exit} = 21$bar $=$ const..
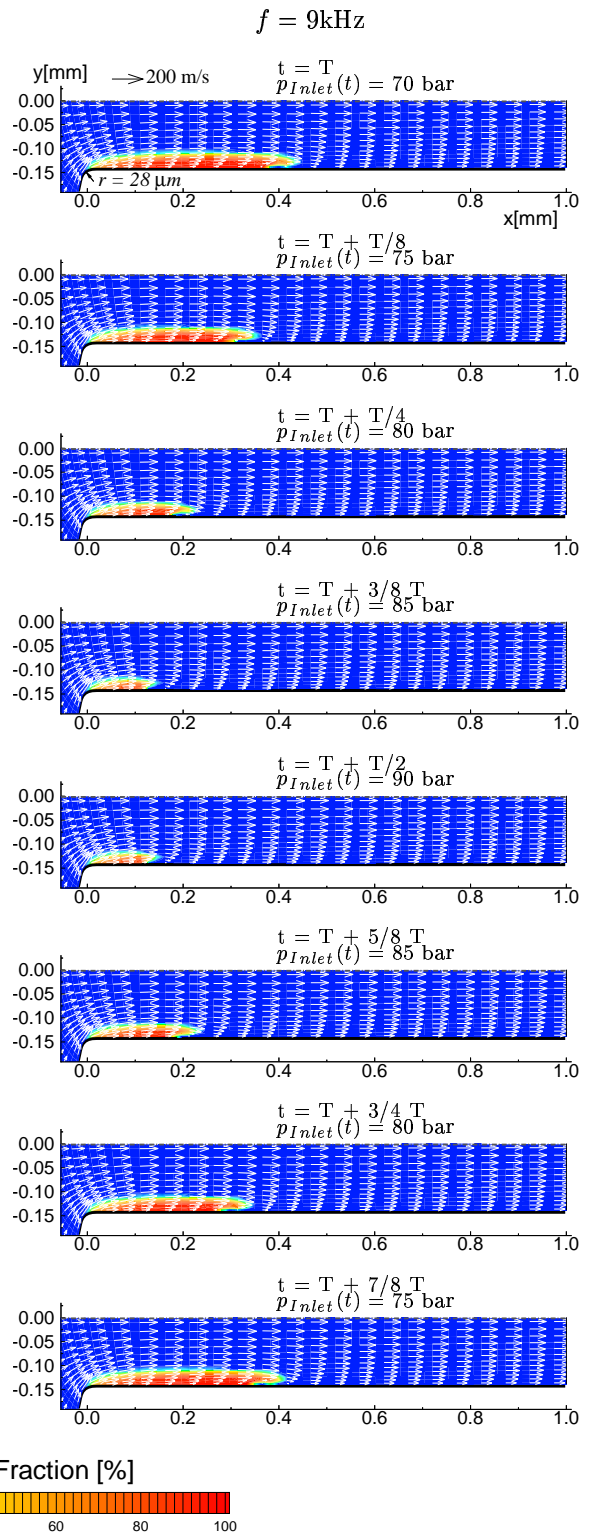
Figure 9: Unsteady periodic vapor fraction distribution, **triangle wave** inlet pressure $p_{Inlet}(t)$, $f = 9$kHz, $p_{Exit} = 21$bar $=$ const..

pressures, in spite of the same frequencies and amplitudes. Accidentally, the cavitation process of a single
cycle in the case with the triangle wave inlet pressure $f = 9\mathrm{kHz}$ looks like that of the case with the square
wave inlet pressure $f = 37\mathrm{kHz}$, see figures 9 and 4. The development of the total vapor volume also confirms
this similarity, see figures 6 and 2, although the frequencies and fluctuation types of the two cases are quite
different. This implies that the overall effects including local effect and convective effect are similar in the
two cases. However, it is difficult to derive a generally accepted similarity law relating the cavitation process
and the flow field.

4   Conclusions

Our numerical model has been used to investigate cavitation processes in an injector nozzle under different
inlet pressure fluctuations. The computed results confirm, that if the injection pressure increases rapidly,
the cavitation simultaneously becomes weaker due to the temporal pressure rise in the nozzle. There exists
a time delay till the cavitation becomes more intense again after the injection pressure has increased and
then remains constant. Furthermore, different types of injection pressure fluctuations influence the extension
of cavitation and the phase shift between the time history of the inlet pressure and the cavitation process.
This unsteady effect indicates that the cavitation process has its own time and length scale. It is necessary
to account for unsteady boundary conditions. Numerical simulation provides a right way to analyze the
unsteady cavitation process.

Acknowledgment

References

Chaves, H., Kirmse, C., Obermeier, F. (2000). The influence of nozzle inlet curvature on unsteady cavitation
in transparent diesel injection nozzles. In *Proc. 1st International Colloquium on Microhydrodynamics* (ed.
J. Fabri). Société Francaise des Mécaniciens, Paris, France.

Chaves, H., Knapp, M., Kubitzek, A., Obermeier, F., Schneider, T. (1995). Experimental study of cavitation
in the nozzle hole of diesel injectors using transparent nozzles. *SAE Paper 950290.*

Chaves, H., Obermeier, F. (1996). Modelling the effect of modulations of the injection velocity on the
structure of diesel sprays. *SAE Paper 961126.*

Grabitz, G., Kubitzek, A., Chaves, H. (1995). Die Rolle der Oberflächenspannung beim Zerfall stark gestörter
Flüssigkeitsfreistrahlen. *Z. angew. Math. Mech.* **75** SI, 383-384.

Hirt, C. W., Nichols B. D. (1981). Volume of fluid (VOF) method for the dynamics of free boundaries.
Journal of Computational Physics **39**, 201-225.

Rayleigh, L. (1917). On the pressure developed in a liquid during the collapse of a spherical cavity. *Phil.
Mag. S. 6*, Vol. 34, No. 200, pp. 94-98.

Roosen, P., Unruh, O., Behmann, M. (1996). Untersuchung und Modellierung des transienten Verhaltens
von Kavitationserscheinungen bei ein- und mehrkomponentigen Kraftstoffen in schnell durchströmten Düsen.
Report of the Institute for Technical Thermodynamics, RWTH Aachen (Univ. of Tech.), Germany.

Schnerr, G. H., Sauer, J. (2001). Physical and numerical modeling of unsteady cavitation dynamics. In
Proc. 4th International Conference on Multiphase Flow. New Orleans, USA.

Spalding, D. B. (1974). A method for computing steady and unsteady flows possessing discontinuities of
density. *CHAM report 910/2.*

Wilcox, D. C. (1998). Turbulence modeling for CFD. DCW Industries, Inc., La Cañada, California, USA.

Yuan, W., Sauer, J., Schnerr, G. H. (2000). Modeling and computation of unsteady cavitation flows in
injection nozzles. In *Proc. 1st International Colloquium on Microhydrodynamics* (ed. J. Fabri). Société
Francaise des Mécaniciens, Paris, France.

Yuan, W., Schnerr, G. H. (2001). Cavitation in injection nozzles - Effect of the unsteady supply pressure.
In *Proc. 5th ISAIF - International Symposium on Experimental and Computational Aerothermodynamics of
Internal Flows*. Institute of Fluid Flow Machinery, Gdansk, Poland.